Quaternary Science Reviews 29 (2010) 3057–3066

Contents lists available at ScienceDirect

Quaternary Science Reviews

journal homepage: www.elsevier.com/locate/quascirev

Geochemical and climate modeling evidence for Holocene aridification in Hawaii: dynamic response to a weakening equatorial cold tongue

Joji Uchikawa [a,*], Brian N. Popp [b,1], Jane E. Schoonmaker [a,2], Axel Timmermann [c,3], Stephan J. Lorenz [d,4]

[a] Department of Oceanography, SOEST, University of Hawaii. 1000 Pope Road, Honolulu, HI 96822, USA
[b] Department of Geology and Geophysics, SOEST, University of Hawaii. 1680 East-West Road, Honolulu, HI 96822, USA
[c] IPRC, SOEST, University of Hawaii. 2525 Correa Road, Honolulu, HI 96822, USA
[d] Max Planck Institute for Meteorology. Bundesstr 55, D-20146, Hamburg, Germany

ARTICLE INFO

Article history:
Received 22 February 2010
Received in revised form
13 July 2010
Accepted 13 July 2010

ABSTRACT

A 13.5 m sequence of Holocene limnic sediments from a sinkhole on Oahu, Hawaii provides a valuable paleoclimatic record for the central subtropical Pacific. $\delta^{13}C$ analysis of plant leaf waxes (*n*-alkanes: *n*-C_{27}, *n*-C_{29}, *n*-C_{31} and *n*-C_{33}) is used to infer vegetative changes. Average $\delta^{13}C$ values of the suite of *n*-alkanes increase from approximately $-31 \pm 0.5‰$ at 10 ca kyr BP (calibrated thousand years before present) to about $-27 \pm 0.5‰$ by 6 ca kyr BP and then remain roughly constant until the Polynesian arrival (about 1.15 ca kyr BP). The increase in $\delta^{13}C$ values of *n*-alkanes is interpreted to indicate a shift in the local vegetation from C_3 to C_4-dominated flora. Based on mass-balance calculations, the observed increase in the $\delta^{13}C$ values translates to at least a doubling of the relative abundance of C_4 plants. We argue that the expansion of C_4 plants was a response to decreased overall water availability (aridification) due to reduced wintertime precipitation. Model simulations of an orbitally-induced increase in insolation along the equator during the Holocene provide evidence for a wintertime drying trend in the eastern subtropical North Pacific. This trend is associated with boreal fall to winter warming of the cold tongue in the eastern equatorial Pacific (EEP). These model results provide a conceptual framework to explain a dynamic link between the reconstructed Holocene drying trend in Hawaii and orbitally-forced climate change in the EEP that is analogous to the modern El Niño-Southern Oscillation teleconnection.

1. Introduction

Although Holocene climate is often characterized as relatively mild and stable, a growing number of studies provide evidence of Holocene climatic variability on various timescales. For example, orbitally-driven changes in the mean meridional positioning of the Intertropical Convergence Zone (ITCZ) caused significant changes in the hydrologic cycles in regions where precipitation is either directly influenced by the ITCZ itself (e.g., Hodell et al., 1991; Haug et al., 2001; Fleitmann et al., 2003, 2007; Shakun et al., 2007; Sachs et al., 2009) or by seasonal monsoons modulated by the ITCZ (e.g., Dykoski et al., 2005; Wang et al., 2005; Yancheva et al., 2007). These records show a general southward shift of the mean latitudinal position of the ITCZ during the Holocene. Superimposed on this trend are high amplitude fluctuations that are particularly pronounced in the late Holocene. Haug et al. (2001) and Peterson and Haug (2006) argued that these signals perhaps reflect strong El Niño-Southern Oscillation (ENSO) forcing. Lacustrine sedimentary records from an alpine lake in Ecuador (Rodbell et al., 1999; Moy et al., 2002) indicate an intensification of ENSO activity since 7 ca kyr BP (calibrated thousand years before present). Meanwhile, more recent lithologic records with higher resolution demonstrate robust El Niño signals (in terms of event intensity and/or frequency) after 5 ca kyr BP or so (Rein et al., 2005; Conroy et al., 2008).

Despite significant contributions from many studies, localities of high-resolution Holocene paleoclimatic proxy records in the Pacific basin are mostly concentrated in the western and eastern margins of the circum-Pacific region (see Donders et al., 2008). In contrast, the vast area of the central tropical/subtropical Pacific still remains a major gap that needs to be filled with robust paleoclimatic records capturing low latitude climate variability. This poses

* Corresponding author. Tel.: +1 808 956 3285; fax: +1 808 956 7112.
E-mail addresses: uchikawa@hawaii.edu (J. Uchikawa), popp@hawaii.edu (B.N. Popp), jane@soest.hawaii.edu (J.E. Schoonmaker), axel@hawaii.edu (A. Timmermann), stephan.lorenz@zmaw.de (S.J. Lorenz).
[1] Tel.: +1 808 956 6206; fax: +1 808 956 5512.
[2] Tel.: +1 808 956 9935; fax: +1 808 956 9225.
[3] Tel.: +1 808 956 2720; fax: +1 808 956 9425.
[4] Tel.: +49 40 41173 156; fax: +49 40 41173 298.

0277-3791/$ – see front matter © 2010 Elsevier Ltd. All rights reserved.
doi:10.1016/j.quascirev.2010.07.014

a major challenge for a systematic understanding of Holocene Pacific climate variability. Because the tropical/subtropical Pacific Ocean represents an enormous source of heat and moisture, reliable proxy records from oceanic locations in low latitudes of the Pacific are particularly valuable in the context of paleoclimatology.

Due to its unique isolation in the central subtropical Pacific, Hawaii is an intriguing location to explore reliable paleoclimatic archives. The first human settlement to the main Hawaiian Islands by the Polynesians occurred around 1.15 ca kyr BP (Athens et al., 2002), which minimizes anthropogenic biases for most of the Holocene. But to date, notable paleoclimatic reconstructions from Hawaii are limited to the work by Lee and Slowey (1999), Lee et al. (2001) and Hotchkiss and Juvik (1999). Lee and Slowey (1999) and Lee et al. (2001) reconstructed sea surface temperature (SST) for the past 30 ca kyr BP based on foraminiferal abundance and alkenone $U^{K'}_{37}$ values from sediment cores collected off Oahu, Hawaii. Their SST records, however, are relatively difficult to utilize in the context of Holocene Pacific paleoclimatology because the corresponding portion of the record is of relatively low resolution. Hotchkiss and Juvik (1999) constructed detailed late-Quaternary pollen records from Ka'au Crater, Oahu, however, the records only extend up to about 7 ca kyr BP. Thus models of climate change in Hawaii throughout the entire Holocene still remain largely elusive.

In this paper, we report the results of a paleoclimatic reconstruction based on the $\delta^{13}C$ values of plant leaf waxes (*n*-alkanes: *n*-C_{27}, *n*-C_{29}, *n*-C_{31} and *n*-C_{33}) extracted from coastal pond sediments from Oahu, Hawaii. The $\delta^{13}C$ values of *n*-alkanes (denoted as $\delta^{13}C_{alk}$ hereafter) are used to infer terrestrial vegetation changes, which in turn reflect paleo-aridity changes. Although interpretation of detailed paleoclimatic fluctuation is limited by the distribution of data and the sediment chronology, these results represent the first continuous Holocene terrestrial paleoclimatic proxy records from Hawaii. Our paleoclimatic reconstruction based on isotopic results is also supplemented with a transient climate model simulation using a coupled general circulation model (CGCM) in order to assess the principle driving mechanism of regional climate change near Hawaii.

2. Environmental settings and descriptions of the sediment core

2.1. Study area

The study site, Ordy Pond, is situated along the leeward coast of the Ewa Plain on the island of Oahu, Hawaii (Fig. 1). This pond represents the only permanent aquatic feature on the arid coastal area of the Ewa Plain. The pond occupies a 22.5 m deep limestone-hosted sinkhole and contains roughly 5 m of highly stratified brackish (22–25 salinity unit) water (Garrison, 2002). The circular rim of the pond is densely colonized by American mangrove (*Rhizophora mangle*) within a mixed shrub of kiawe trees (*Prosopis pallida*) and sourbush (*Pluchea symphytifolia*) (Athens et al., 2002). The pond was transformed into an aquatic system around 10 ca kyr BP as groundwater inundated the open sinkhole during the most recent post-glacial sea level rise. Today the pond receives no permanent surface inflow and appears to be largely isolated from the surrounding aquifer. Episodic seasonal rainfall events and perhaps extremely limited groundwater intrusions are the only sources of water to the pond system. Further descriptions of Ordy Pond and the surrounding environment of the Ewa Plain are provided elsewhere (Tribble et al., 1999; Athens et al., 2002; Garrison, 2002; Athens, 2008; Uchikawa et al., 2008).

The blockage of the persistent moisture-laden northeasterly trade winds by the Koolau Mountain range, which spans from the northernmost to the southeastern end of the island, creates areas of rain-shadow over much of the leeward low-lands of Oahu. Annual precipitation on the Ewa Plain is therefore limited. Average annual precipitation between 1949 and 2001 was 508 mm, but most notably, an average of 381 mm fell during winter months (from October to March). On the leeward side of the main Hawaiian Islands, much of the winter precipitation (and thus annual precipitation) can be contributed by a few torrential downpours associated with winter cyclonic storms, locally known as Kona Lows (Otkin and Martin, 2004). Furthermore, precipitation in Hawaii is characterized by significant interannual variability. During El Niño events, prolonged droughts prevail due to reduction in large-scale moisture supplies (Chu, 1995) as well as reduced probability of Kona Lows (Chu, 1995; Rooney and Fletcher, 2005; Caruso and Businger, 2006). Daily rainfall records collected since 1949 at the NAS Barbers Point weather station, which is in close proximity to Ordy Pond, indicate an average precipitation of 1.2 mm/day in El Niño years and 2.0 mm/day in La Niña years (NOAA [http://cdo.ncdc.noaa.gov]).

2.2. Description of the sediment core

A 17.5 m long sediment core collected from Ordy Pond contains roughly 13.5 m of limnic sediments overlying 4 m of terrigenous debris from the base of the sinkhole. The absence of obvious hiatuses and unconformities in the limnic sediments suggests

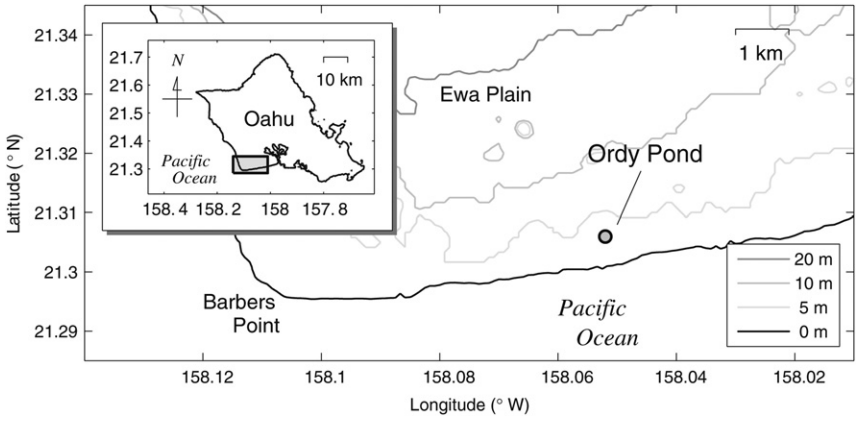

Fig. 1. Coastal topography of the Ewa Plain of Oahu, Hawaii. The study site, Ordy Pond, is approximately 750 m from the coastline and situated at about 1.5 m above current mean sea level. The size of the pond (roughly 0.5 ha) is exaggerated in this map.

continuous deposition throughout the Holocene since the initial inundation of the open sinkhole around 10 ca kyr BP (Tribble et al., 1999; Uchikawa et al., 2008). The upper 5.2 m of the limnic sediments, representing the most recent 170 years of sedimentation, consist of organic-rich sapropels. Comparatively high sedimentation rate in this sedimentary interval is most likely due to significant land-use change such as cattle ranching and commercial agriculture on the Ewa Plain during this era (Garrison, 2002). The lower 8.2 m of the sediments show characteristic fine-scale laminations (mm to cm scale) with alternating layers that are rich in authigenic carbonates and/or diatom tests (light-colored layers) and organic matter (dark-colored layers). Further descriptions of the sediment core are summarized elsewhere (Tribble et al., 1999; Garrison, 2002; Uchikawa et al., 2008).

Establishment of reliable age control for Ordy Pond sediments has been extremely challenging because of scarcity of datable materials and unknown radiocarbon reservoir effects in the pond system (see Uchikawa et al., 2008 for details). Uchikawa et al. (2008) conducted compound-specific radiocarbon dating on *n*-alkanes extracted from the bulk sediments to circumvent these problems. The most recent age model (Fig. 2) by Uchikawa et al. (2008) utilizes these newly derived radiocarbon dates from *n*-alkanes as well as several radiocarbon dates based on rare plant macrofossils and an archaeological date by Athens et al. (2002). The model is well constrained for the upper 9 m of the core, which dates back to approximately 2.5 ca kyr BP. But the chronology for deeper and older part of the sedimentary sequence has large uncertainty because of the coarse age resolution and inconsistency in the radiocarbon dates based on plant macrofossils and *n*-alkanes.

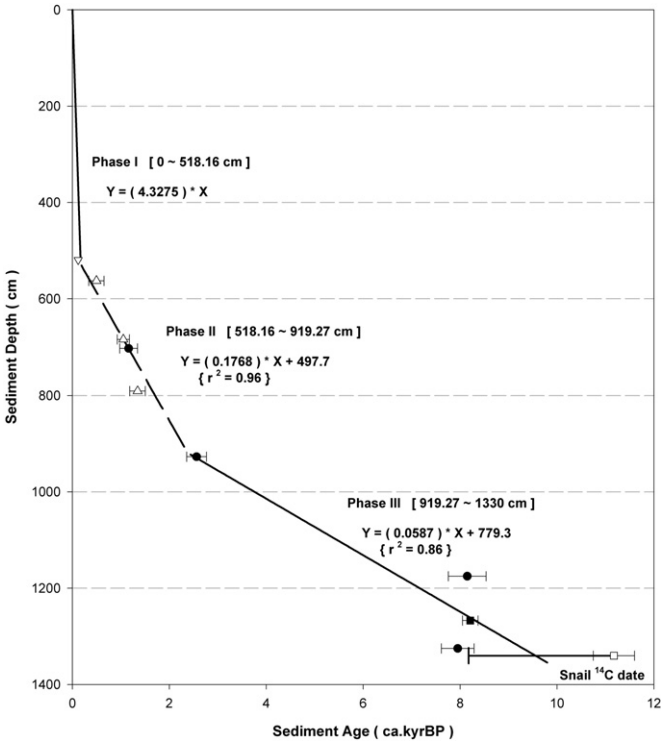

Fig. 2. Current age control for Ordy Pond limnic sediments (modified from Uchikawa et al., 2008). Open triangles represent the dates from Athens (1997) and Athens et al. (2002). Downward triangle is the date based on archaeological evidence and upward triangles are radiocarbon dates on plant macrofossils. Filled symbols represent the radiocarbon dates based on *n*-alkanes (circles) and a wood fragment (square) by Uchikawa et al. (2008). The error bars on the radiocarbon dates represent combined uncertainty associated with the radiocarbon analyses and calibration with the CALIB program. The age models for three distinct sedimentation phases are based on linear interpolation and linear regression of these dates (see the equations in the figure. Y: sediment depth in cm, X: sediment age in ca yrBP). Note that the radiocarbon date on terrestrial snail shells (open square; Tribble et al., 1999) was not used for the age model. This is because radiocarbon dates of snail shells from limestone areas are often erroneously "too old" due to the incorporation of ^{14}C-depleted carbon. In order to demonstrate the uncertainty associated with the "limestone effect", the snail radiocarbon date is supplemented with a conceptual error bar of 3000 years (see Uchikawa et al., 2008 for details).

3. Methods

3.1. Analytical methods

The methods for the isolation of *n*-alkanes from sediments are thoroughly described in Uchikawa et al. (2008). Briefly, oven-dried (60 °C) bulk sediment samples were soxhlet-extracted with dichloromethane. Elemental sulfur was removed from the lipid extracts using acid activated granular copper. The hydrocarbon fraction in the extracts was separated by silica-gel column chromatography. Finally the *n*-alkane fractions were isolated from the hydrocarbon fraction using silicalite molecular sieve (Kenig et al., 2000).

Compound-specific δ^{13}C analyses of the individual *n*-alkanes (*n*-C_{27}, *n*-C_{29}, *n*-C_{31} and *n*-C_{33}) were performed by isotope-ratio-monitoring GC/MS (MAT252 with GC/C-III interface). The *n*-alkane fraction was injected using a cold on-column injector onto a J&W DB-1 capillary column (60 m, 0.32 mm i.d., 0.25 μm film thickness) and the individual compounds were separated by increasing the GC oven temperature from 50 °C to 320 °C at a rate of 4 °C/min and holding the temperature at 320 °C for 20 min thereafter. A suite of deuterated *n*-alkanes (*n*-C_{24}, *n*-C_{36} and *n*-C_{40}) with known δ^{13}C values was co-injected with the samples in order to assess analytical precision and accuracy. The results of the isotopic analyses were standardized to the VPDB scale. Precision and accuracy was generally better than ± 0.3‰, except for a few samples (up to ± 0.6‰, see Table 1).

Approximately 1–2 cm of sediment interval (corresponding to 2–3 g of dry sediments) was required for each sample to extract sufficient quantities of *n*-alkanes for at least duplicate compound-specific δ^{13}C analyses. Considering the abundant sediment laminae bracketed within a sampling interval, each sample is expected to represent the time-averaged signal of vegetation change of up to decades.

3.2. Descriptions of the coupled general circulation model (CGCM)

The CGCM used in this study is the global atmosphere-ocean-sea ice model ECHO-G (Legutke and Voss, 1999; Min et al., 2005). The ocean and atmosphere components of the model are HOPE-G and ECHAM4 (Roeckner et al., 1996), respectively (see Lorenz et al., 2006 and Timmermann et al., 2007 for details). Constant greenhouse gas concentrations (CO_2: 280 ppm, CH_4: 700 ppb and N_2O: 264 ppb) for the preindustrial era were prescribed in the model. Surface background albedo, vegetation ratio, leaf area index, distribution of continents and oceans and orographic forcing were kept constant at their present values throughout the simulation. To avoid strong model drift, the coupled model runs were performed with annual mean flux correction fields for both heat and freshwater fluxes. The seasonal cycle was not flux-corrected. The ENSO performance of this model is described in detail in Min et al. (2005).

With this CGCM a long-term simulation was performed corresponding to the time from 142 kyr BP (kyr BP: thousand model-simulation years before present) up to 22.9 kyr AP (AP: after present) (Felis et al., 2004; Timmermann et al., 2007). The climate was driven by a changing seasonal distribution of incoming solar radiation (insolation) due to the evolution of the parameters of the

Table 1
$\delta^{13}C$ values of individual *n*-alkanes extracted from Ordy Pond sediments and estimated fractional abundance of C_4 plants based on isotope mass-balance calculations (see text for details).

Depth (cm)	Age (ca.kyrBP)	$\delta^{13}C$[a] *n*-C_{27}	$\delta^{13}C$[a] *n*-C_{29}	$\delta^{13}C$[a] *n*-C_{31}	$\delta^{13}C$[a] *n*-C_{33}	Analytical Uncertainty (‰)	Weighted Mean (‰)	% C_4 Abundance (Weighted Mean)	% C_4 Uncertainty (%)
492	0.11	−23.54	−26.6	−25.31	−22.86	±0.66	−24.58	79.0	± 9.3
525	0.13	−21.25	−24.16	−23.53	−22.86	±0.24	−22.95	88.2	± 9.0
564	0.36	−20.5	−23.42	−23.93	−22.26	±0.13	−22.53	90.1	± 8.9
590	0.51	−25.18	−27.92	−26.23	−22.78	±0.24	−25.53	74.2	± 9.2
598	0.55	−25.25	−26.79	−26.74	−23.71	±0.66	−25.6	72.0	± 9.4
640	0.79	−23.26	−25.6	−26.59	−25.78	±0.65	−25.31	70.8	± 9.4
651	0.85	−27.04	−28.63	−27.10	−26.70	±0.24	−27.37	60.5	± 9.4
686.5	1.06	−26.47	−27.62	−26.30	−27.78	±0.24	−27.04	61.8	± 9.4
702	1.15	−28.22	−25.59	−26.59	−25.48	±0.10	−26.47	67.3	± 9.2
740	1.36	−25.87	−28.47	−25.74	−27.12	±0.13	−26.80	64.2	± 9.3
786.5	1.63	N/A	−29.40	−26.66	−28.30	±0.66	−28.12	56.9	± 10.4
850	2.00	−27.10	−28.96	−26.69	−27.32	±0.24	−27.52	59.7	± 9.4
927	2.52	−26.48	−28.30	−26.62	−27.11	±0.50	−27.13	61.6	± 9.5
975	3.33	−26.28	−27.58	−26.50	−27.67	± 0.65	−27.01	61.7	± 9.6
1017	4.05	−27.44	−28.31	−28.06	−28.92	±0.24	−28.18	53.2	± 9.6
1060	4.78	−23.22	−23.82	−24.85	−24.91	±0.65	−24.20	79.1	± 9.3
1107	5.58	−25.33	−26.98	−26.69	−27.17	±0.30	−26.54	63.8	± 9.4
1140	6.14	−25.15	−25.66	−27.55	−28.53	±0.65	−26.72	60.8	± 9.7
1175	6.74	−26.98	−29.00	−29.84	−28.54	±0.43	−28.59	49.2	± 9.8
1195	7.08	−27.77	−28.63	−29.33	−28.77	±0.65	−28.63	49.6	± 9.9
1240	7.85	−27.05	−29.15	−28.31	−27.98	±0.24	−28.12	53.9	± 9.6
1285	8.61	−27.17	−28.91	−29.94	−29.22	±0.27	−28.81	47.4	± 9.8
1325	9.30	−27.63	−29.86	−31.87	−31.79	±0.24	−30.29	35.7	± 10.2
1335	9.47	−29.29	−31.17	−33.26	−31.98	±0.24	−31.43	28.6	± 10.4
1362.5	9.94	−29.53	−30.49	−32.32	−31.69	±0.13	−31.01	32.1	± 10.3

[a] In ‰ unit, VPDB scale.

earth's orbit around the sun (following Berger, 1978). To capture this long time span, orbital forcing was applied with a time acceleration factor of 100 (see Lorenz and Lohmann, 2004). Under the model setting described above, SST (particularly in the tropical oceans) adjusts to insolation changes within 2–4 months. This helps to set up SST gradients, which ultimately drive wind changes and feedback onto the SST evolution. Thus, we expect the tropical oceans to be in quasi-equilibrium even with the accelerated orbital forcing. The maximum rate of insolation change in the accelerated model run was less than 1 $W/m^2/yr$. Our analysis focuses only on the period from 20 kyr BP to 20 kyr AP. It should be noted that these CGCM experiments are not simulations of the "real" climate evolution since 20 kyr BP. Instead, these experiments represent sensitivity runs to address the effects of varying insolation signal due to the changing orbital parameters. As a final remark, the reliability of the ECHO-G simulation was verified by transient ensemble simulations (Lorenz et al., 2006), which documented a good correspondence with alkenone-derived SST records.

4. Results and discussions

4.1. Results of isotopic analyses

Leaf wax *n*-alkanes were ubiquitous in Ordy Pond sediments. A long-chain odd-carbon-numbered homologous series ranging from *n*-C_{25} to *n*-C_{35} dominated the *n*-alkanes extracted from sediments. The most quantitatively abundant compound in each sample was either *n*-C_{29} or *n*-C_{31}. The $\delta^{13}C$ values of *n*-alkanes ($\delta^{13}C_{alk}$) vary between a low of −33.26‰ and a high of −20.5‰ through the 13.5 m core (Table 1). Table 1 also demonstrates that there are differences in the $\delta^{13}C_{alk}$ values among the four individual *n*-alkanes in each sample. But these individual compounds provide very similar overall trends of change in the $\delta^{13}C_{alk}$ values over time. We therefore report the results in Fig. 3a using the weighted mean $\delta^{13}C$ values computed from the isotopic results of *n*-C_{27}, *n*-C_{29}, *n*-C_{31} and *n*-C_{33} (weighting is based on the analytical reproducibility, see Fig. 3 caption).

The weighted mean $\delta^{13}C_{alk}$ values (Fig. 3a) increase from roughly −31‰ at 10 ca kyr BP to −27‰ at 6 ca kyr BP and then remain more or less constant until the beginning of human settlement (1.15 ca kyr BP: Athens et al., 2002). The only exception to this overall pattern is the anomalous data point indicating the highest $\delta^{13}C$ value (as high as −24‰) of the record prior to the human settlement. This data point is tentatively dated at 4.8 ca kyr BP based on our current sediment age model. In samples deposited after the Polynesian settlement in the main Hawaiian Islands (1.15 ca kyr BP), the weighted mean $\delta^{13}C_{alk}$ values increase from about −27‰ to −23‰ with decreasing age.

4.2. Interpretation of the isotopic results

Our $\delta^{13}C_{alk}$ record most likely reflects changes in vegetative structure over time. $\delta^{13}C$ values of *n*-alkanes synthesized by C_3 and C_4 plants range from −28 to −40‰ and from −17 to −25‰, respectively (Collister et al., 1994; Chikaraishi and Naraoka, 2003; Bi et al., 2005). The observed changes in our Holocene $\delta^{13}C_{alk}$ record (Fig. 3a) is interpreted to reflect the shift in the relative abundances of C_3 (primarily trees and shrubs) and C_4 species (mostly grasses) in response to climate shifts and/or other factors.

Distributions of C_3 and C_4 plants are controlled by the combined effects of the atmospheric CO_2 level (pCO_2), temperature and water availability (Ehleringer, 2005). C_4 photosynthesis is more efficient than the C_3 counterparts under low pCO_2 levels due to a carbon concentrating mechanism. In contrast, increasing pCO_2 levels should favor the ecological success of C_3 plants (Ehleringer et al., 1997; Keeley and Rundel, 2003). But our *n*-alkane record shows expansion of C_4 plants during the Holocene, during which the pCO_2 steadily rose by 20 ppm (Indermühle et al., 1999). This mismatch suggests that pCO_2 was not the dominant selective factor for the local vegetation.

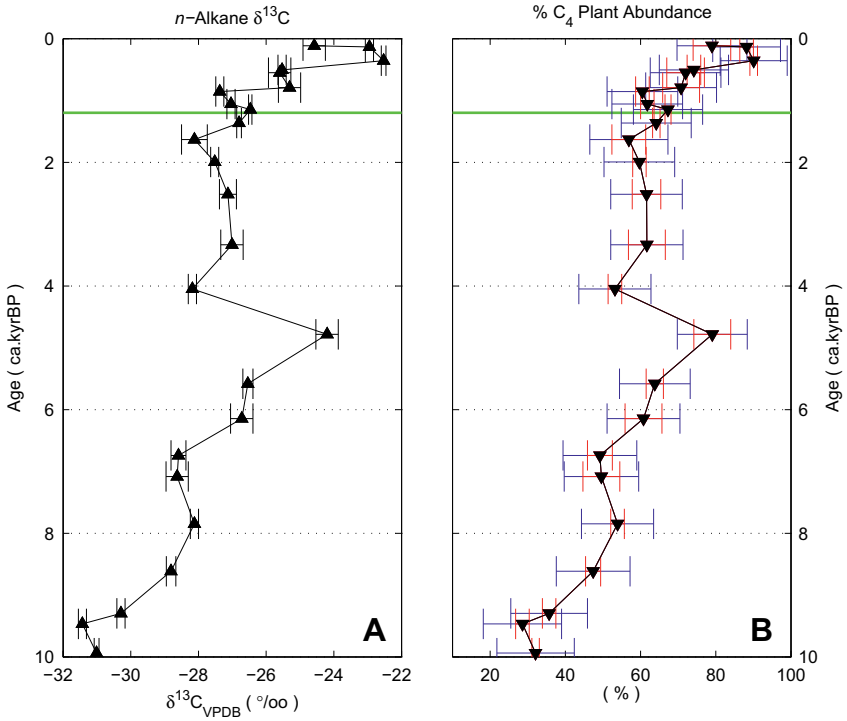

Fig. 3. (A) Weighted mean $\delta^{13}C$ values of individual *n*-alkanes extracted from Ordy Pond sediments as a function of age (weighted mean = $\{\sum(\delta_i/\sigma_i^2)\}/\{\sum(1/\sigma_i^2)\}$; standard deviation = $\{\sum(1/\sigma_i^2)\}^{-0.5}$). Weighting was based on the analytical reproducibility of the isotopic analyses. (B) Variation in the fractional abundance of C_4 plants as a function of age. Values are the weighted means of four separate estimates based on $\delta^{13}C$ value of *n*-C_{27}, *n*-C_{29}, *n*-C_{31} and *n*-C_{33}. Smaller error bars in red represent the probable ranges of errors in the estimates due to the reproducibility of the isotopic analyses. Larger error bars in blue denote combined errors (due to the analytical reproducibility and the uncertainties in the end-member $\delta^{13}C$ values: see Table 2). The solid line at 1.2 ca kyr BP marks the estimated time of the first human arrival in Hawaii (Athens et al., 2002).

C_3/C_4 plant distributions are sensitive to temperature during the growth period. Cool and warm growth periods promote the dominance of C_3 and C_4 plants, respectively (Ehleringer, 2005). It is also known that under limited water availability, C_4 plants are favored due to superior water use efficiency and high photosynthetic rates even upon stomatal closure (Stowe and Teeri, 1978; Ehleringer et al., 1997; Epstein et al., 1997; Keeley and Rundel, 2003). On the basis of indirect evidence, we argue that temperature exerted relatively insignificant control on C_3/C_4 plant distributions compared to the water availability in the vicinity of the study site. The SST reconstruction by Lee et al. (2001) based on marine sediment cores collected from Oahu's southwest coastline shows only minor (1 °C at most) fluctuations of both summer and winter-averaged SST during the Holocene. Considering the proximity of our study site to the ocean (about 750 m) and to the locations where their marine sediment cores were collected (see Fig. 1 in Lee et al., 2001), overall changes in the ambient temperature as well as in the seasonal temperature difference (summer vs. winter) during the Holocene are expected to have played only a minor role. In contrast, the pollen records of Hotchkiss and Juvik (1999) from Ka'au Crater indicate noticeable reduction in the precipitation from 10 to 7 ca kyr BP on Oahu, but no apparent changes in ambient temperature. Furthermore, Edwards and Still (2008) reviewed the distribution of modern C_3 and C_4 plants in Hawaii and suggested that the higher water use efficiency of the C_4 plants is more important than temperature in controlling the distribution of C_3 and C_4 grasses. In addition, a study of vegetation history before Polynesian settlement along an elevational transect in the leeward coast of Kohala volcano, Hawaii, by Chadwick et al. (2007) further supports the overlying importance of water availability in influencing the zonation of C_3 and C_4 plants. Results from their lower elevation sites (77–992 m), which cover a wide range of mean annual precipitation (170–1120 mm), but a relatively narrow range of mean annual temperature (23–19 °C), show a continuous shift of relict vegetation from a C_3 to C_4-dominated system with decreasing precipitation. In summary, the results of studies of modern and Holocene Hawaiian vegetation along with evidence for a lack of growing season temperature changes at our study site argue for a causal link between the dominance of C_4 photosynthesis and precipitation on the Ewa Plain.

It should be noted that the shift to higher $\delta^{13}C_{alk}$ values in our record may also reflect a physiological control on the extent of isotopic discrimination against $^{13}CO_2$ during C_3 photosynthesis. The extent of ^{13}C discrimination varies linearly with the ratio between intercellular and atmospheric CO_2 partial pressure (p_i/p_a), which is regulated by the degree of stomatal opening (Farquhar et al., 1989; Ehleringer et al., 2002). Stomatal closure in response to water stress raises the water use efficiency but decreases the p_i/p_a ratio. This results in a greater assimilation of $^{13}CO_2$ and consequently ^{13}C enrichment in plant tissues, including leaf wax *n*-alkanes (Lockheart et al., 1998). The p_i/p_a ratios of C_3 plants vary from 0.5 to 0.8 (Ehleringer et al., 2002), resulting in variations of $\delta^{13}C$ up to 7‰ in C_3 plants. As an example, Austin and Vitousek (1998) observed about 4‰ ^{13}C enrichment in the C_3 plants *Metrosiderous polymorpha* along a precipitation gradient (5500–500 mm in mean annual precipitation) on the island of Hawaii.

It is not possible to distinguish the causes (vegetation shifts vs. changes in isotopic fractionation during C_3 photosynthesis) of the observed changes in $\delta^{13}C_{alk}$ values based on our isotopic results. But it is important to note that both scenarios suggest that the positive shift in $\delta^{13}C_{alk}$ values reflects an increase in aridity (decreased moisture). We favor the interpretation that the changes in $\delta^{13}C_{alk}$ values reflect vegetative shifts between C_3 to C_4-dominated flora because the range of observed $\delta^{13}C_{alk}$ values (roughly −32‰

to −23‰) exceeds the observed physiological carbon isotopic variations in C_3 plants (up to 7‰). Based on this assumption, the advent/decline of C_3 and C_4 plants can be assessed by isotope mass-balance. Because we are not aware of any published data on the $\delta^{13}C$ values of *n*-alkanes synthesized by indigenous Hawaiian plants, we compiled $\delta^{13}C_{alk}$ values from a variety of living specimens reported in the literature (Collister et al., 1994; Chikaraishi and Naraoka, 2003; Bi et al., 2005) to establish the C_3 and C_4 end-member $\delta^{13}C_{alk}$ values (Table 2). Contemporary geographic distributions of the specimens listed in these studies were inspected using the U.S. Department of Agriculture Plant Database [http://plants.usda.gov]. The $\delta^{13}C_{alk}$ data of plant species that are not found in Hawaii were removed from the data compilation. In contrast, the $\delta^{13}C_{alk}$ data from species with confirmed existence in Hawaii (although neglecting the fact that these are all introduced species) were averaged for the end-member values. This process reduced the standard deviations for the end-member values. The standard deviations of the end-member $\delta^{13}C$ values as well as analytical uncertainties of compound-specific $\delta^{13}C$ analyses were propagated through the mass-balance calculations (see Phillips and Gregg, 2001). Weighted means of estimates based on the individual *n*-alkanes are expressed in % units (% C_4 abundance, hereafter) and listed in Table 1. A typical value for the uncertainties in the estimates of % C_4 abundance is on the order of 10% (Table 1 and Fig. 3b), and much of that is contributed by relatively large uncertainty in the end-member isotopic values (Table 2) due to intra-species and ontogenetic variations in the compiled data.

4.3. Holocene paleo-aridity changes in Hawaii

The *n*-alkane record shows a substantial expansion of C_4 plants (increase of the % C_4 abundance roughly from 30% to 60%) from 10 to 6 ca kyr BP (Fig. 3b), which suggests a reduction in the overall water availability for local vegetation. The reconstructed shift to more arid conditions from early to mid Holocene is consistent with Hawaiian paleo-records covering discrete Holocene time-intervals. Although the record extends only up to 7 ca kyr BP, the pollen records from Ka'au Crater similarly suggests decreasing precipitation on Oahu (Hotchkiss and Juvik, 1999). A paleoenvironmental investigation conducted on Laysan Island in the remote Northwestern Hawaiian archipelago (roughly 1200 km from Oahu) also found evidence of a drying trend since 7 ca kyr BP (Athens et al., 2007).

A maximum C_4 abundance of roughly 80% (tentatively dated at 4.8 ca kyr BP based on the current age model) is an intriguing, albeit limited, feature in this record. The existence of a prolonged (potentially centurial to millennial scale) dry episode centered sometime between 4 and 5 ca kyr BP in Hawaii has been repeatedly advocated based on pollen records from numerous locations on Oahu (Athens, 1997) and Laysan Island (Athens et al., 2007) and charcoal records from several sites on the island of Kauai (Burney and Burney, 2003). Increased sampling resolution in the record and improvement in the sediment chronology are required in order to better characterize this maximum % C_4 signal and the possible link to the dry episode revealed by other terrestrial records from Hawaii.

After the first Polynesian settlement in Hawaii, the record shows dramatic expansion of C_4 plants. But this signal is expected to be decoupled from climatic forcing. Archaeological investigations in the Ewa Plain by Athens et al. (2002) and Athens (2008) revealed abrupt destruction of native forest by human activities and, to a greater extent, by the invasive Polynesian rat (*Rattus exulans*). These environmental disturbances probably provided an open niche for C_4 grasses to quickly expand. Therefore, the post-human portion of the sediments appears to record the vegetative response to human landscape modification rather than paleoclimate.

Based on current seasonal distributions of rainfall and vegetation growth, we argue that the paleoclimatic signals deduced from our *n*-alkane record are biased toward winter climate signals. In other words, the transition toward C_4-dominated flora appears to be a response to decreased overall water availability that is largely pronounced as a decline in wintertime precipitation. Due to the lack of permanent fluvial transport to Ordy Pond, the main transport pathway of leaf waxes to the pond is likely eolian transport. Leaf waxes are thought to be routinely eroded from leaf surfaces by wind abrasion and become airborne (Conte et al., 2003). Although the replacement of eroded leaf waxes occurs regularly (Hallam, 1970), active secretion and replenishment of leaf waxes occur primarily during the early growth phase of emerging leaves (Wirthensohn and Sedgley, 1996; Hauke and Schreiber, 1998). In the arid leeward coastal low-lands of the main Hawaiian Islands, such as the Ewa Plain, vigorous leaf growth (when significant input of *n*-alkanes to the pond is expected) occurs in response to increased rainfall during the boreal winter months (Wagner et al., 1990). In fact, significant greening of the foliage in the local vegetation is recognized during the winter months in the Ewa Plain. Thus, our isotopic record is expected to be dominated by the winter climate signal.

4.4. CGCM simulations

To document the effects of orbital forcing on tropical Pacific climate, the simulated zonally-averaged (from 180 to 120°W) boreal winter SST, surface wind and precipitation anomalies are shown in Fig. 4. Here, we focus on the boreal winter season, because this is the rainy season in Hawaii that will affect leeward vegetation most effectively and because the teleconnections from the eastern tropical Pacific to the Hawaiian Islands are most strongly pronounced (Chu, 1995). From 10 kyr BP to the present, the simulated SST profile shows a continuous winter warming of the equatorial cold tongue (Fig. 4a: also see Fig. 5 in Lorenz et al., 2006). This is accompanied by an intensification of the Hadley circulation and surface trade winds in the northern subtropics, which in turn results in strengthened large-scale atmospheric subsidence. These changes in the surface wind pattern strongly reduce the transport of moist tropical air to Hawaii, leading to an overall drying trend (Fig. 4b). Continuous increase in the winter insolation along the equator throughout the Holocene (Fig. 4c) is the ultimate driver for the observed warming of the cold tongue (Lorenz et al., 2006).

The effect of a general climatic shift due to the warming of the cold tongue in the boreal winter during the Holocene can be compared to the present climatic anomalies around Hawaii associated with an El Niño event. Chu (1995) illustrates that the

Table 2
List of the end-member $\delta^{13}C$ values of the *n*-alkanes synthesized by C_3 and C_4 plants.

	C_3 Plants			C_4 Plants		
	$\delta^{13}C$ (‰)[a]	Std. Dev.	N	$\delta^{13}C$ (‰)[a]	Std. Dev.	N
n-C_{27}	−34.8	±3.4	14	−21.6	±3.5	8
n-C_{29}	−35.9	±2.2	18	−20.9	±3.2	8
n-C_{31}	−36.4	±1.8	19	−20.9	±2.2	9
n-C_{33}	−36.6	±2.3	14	−22.1	±2.3	6

Original data are from Collister et al. (1994), Chikaraishi and Naraoka (2003) and Bi et al. (2005).
See text for the selection criteria for the data compilation for the end-member $\delta^{13}C_{alk}$ values.
Sample code for the compiled data from Collister et al. (1994) (see Table 1 in the original for the codes). [C_3]: D, H [C_4]: X, Z.
Sample code for the compiled data from Chikaraishi and Naraoka (2003) (see Table 1 in the original for the codes). [C_3]: AJ, TO, PA, ArP, MU [C_4]: ZM, SO1, SO2, SB.
Sample code for the compiled data from Bi et al. (2005) (see Table 1 in the original for the codes). [C_3]: D, G, H, J, K, L, M, N, P, Q, R, S [C_4]: T, V, Z.
[a] VPDB Scale.

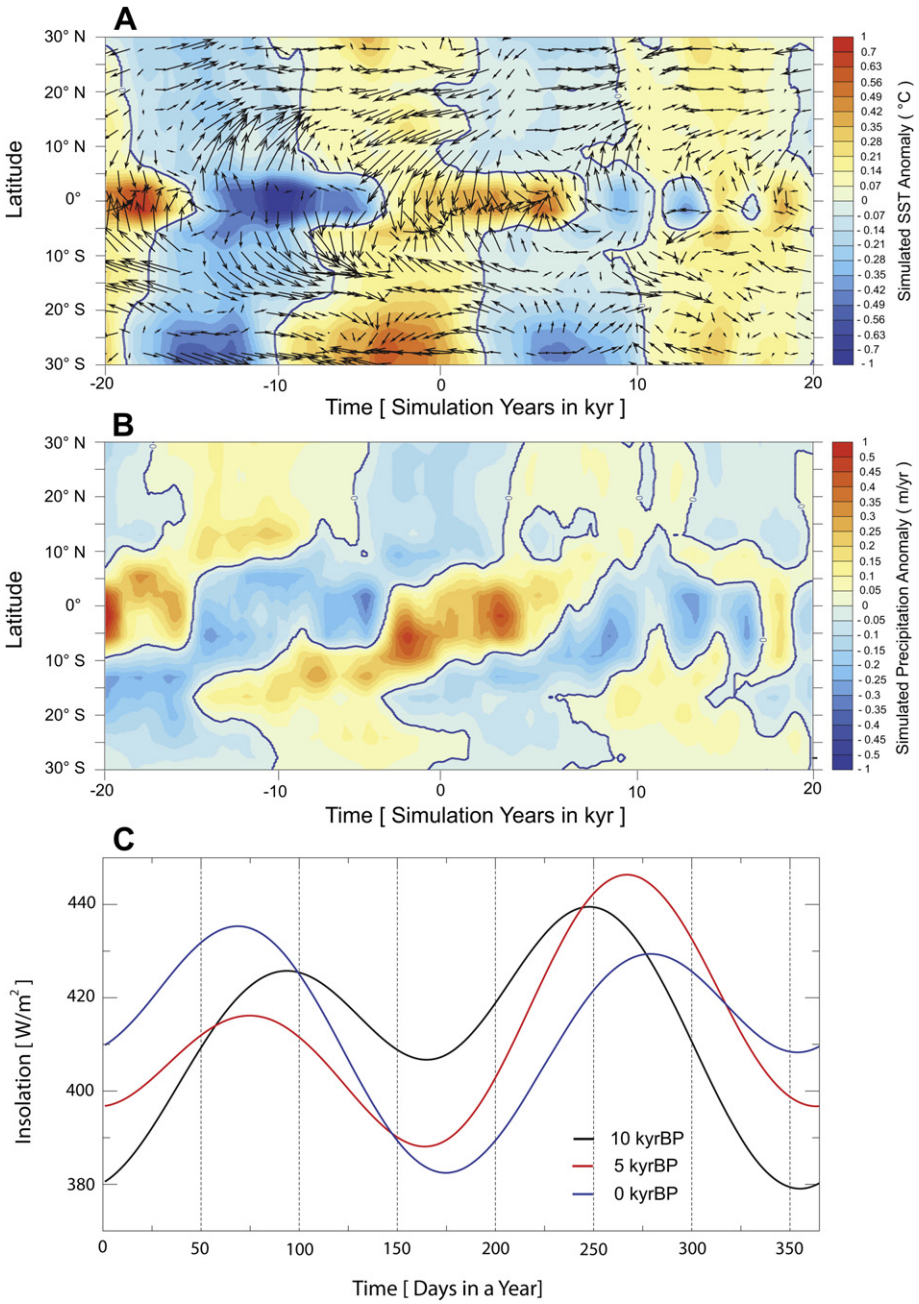

Fig. 4. (A) Simulated boreal winter (DJF) zonally-averaged (180–120 °W) eastern Pacific SST (°C) and 10 m wind anomalies. Anomaly refers to the difference between the zonally-averaged estimates at any given time and the zonally-averaged mean from 20 kyrBP to 20 kyrAP. (B) Same as above, but for the simulated precipitation anomalies (m/yr). (C) Seasonal cycle of insolation (W/m^2) at equator for 10, 5, 0 kyrBP.

large-scale atmospheric circulation changes associated with an El Niño event are mainly driven by an eastward shift of the warm pool and the attendant convection systems toward the equatorial central Pacific, leading to an enhancement of local Hadley circulation as well as increased atmospheric divergence due to southward/eastward displacement of the subtropical jet stream. These atmospheric conditions reduce large-scale moisture supply to the vicinity of Hawaii during an El Niño. Furthermore the probability of subtropical cyclones (Kona Lows) that often deliver large amounts of rainfall to Hawaii during the winter appears to be suppressed during El Niño (Chu, 1995; Caruso and Businger, 2006; Rooney and Fletcher, 2005). Precipitation events from Kona Lows are particularly important for the leeward side of the main Hawaiian Islands as they can contribute over two-thirds of the annual rainfall (Otkin and Martin, 2004). These aspects clearly demonstrate the importance of SST anomalies in the EEP in modulating hydrological conditions near our core site, thus affecting the local vegetation. It should be noted that the CGCM used here is not able to simulate Kona Lows realistically. This suggests that perhaps the simulated winter drying in the subtropical North Pacific due to the weakening of the cold tongue may well be underestimated.

Fig. 4 further illustrates that the warming trend in the equatorial Pacific during the Holocene is part of a larger oscillatory pattern with precessional timescales. The eastern equatorial SST and the simulated equatorial wind divergence vary on a precessional timescale corresponding to the orbitally-controlled seasonal insolation changes (Berger, 1978). Our model results (Fig. 4b) also show opposite precipitation trends in the equatorial zone (increasing

precipitation) and in the northern subtropics (decreasing precipitation). Observed precipitation asymmetry can be explained by the Walker and Hadley circulation adjustments, respectively. While the warming of the cold tongue leads to a weakening of the Walker circulation and an eastward shift of the convection system and the associated precipitation band, an equatorially-forced intensification of the Hadley circulation is responsible for the large-scale subsidence and drying trend in the northern subtropics. It should also be noted that the Holocene drying trend at 10–30°N is also identified in the CGCM simulation for the boreal fall season.

4.5. Synthesis of model results and proxy records

Our paleoclimatic reconstruction based on $\delta^{13}C$ values of leaf wax *n*-alkanes indicates diminished wintertime (and thus the overall annual) precipitation during the mid and late Holocene than in the early Holocene. This is consistent with the results from our model simulations, which demonstrate a concomitant orbitally-forced warming of the cold tongue in the EEP. Reconstructed Holocene changes in the precipitation pattern in Hawaii appear to be a dynamic response to the weakening of the cold tongue in the EEP via large-scale atmospheric adjustments that are similar to the modern-day El Niño-Southern Oscillation teleconnection. In particular, reduced moisture supply via intensified local Hadley circulation and suppression of Kona Lows appear to be the dominant causes for the aridification in Hawaii.

The weakening of the cold tongue throughout the Holocene is consistent with the paleo-SST reconstruction based on alkenone saturation index ($U^{K'}_{37}$) in the EEP (Kienast et al., 2006; Leduc et al., 2007; Pahnke et al., 2007; Koutavas and Sachs, 2008; Dubois et al., 2009). These alkenone SST records are compiled in Fig. 5. Steinke et al. (2008) suggest that $U^{K'}_{37}$-based SST reconstructions are expected to be weighted toward winter-biased signals owing to the seasonal habitat preference of alkenone-producing coccolithophores. Therefore, these alkenone SST estimates may suggest that the weakening of the cold tongue was particularly pronounced during the boreal winter season.

In addition to more direct forcing due to increased winter insolation along the equator (Lorenz et al., 2006), it is plausible that the warming of the cold tongue was also reinforced by the dynamic feedback mechanism in the EEP in response to the southward shift of the mean position of the ITCZ throughout the Holocene (Fig. 5c: Hodell et al., 1991; Haug et al., 2001; Fleitmann et al., 2003, 2007; Shakun et al., 2007). Koutavas and Lynch-Stieglitz (2003,2004) argued that the interactions between the ITCZ and the cold tongue involve positive ocean-atmosphere interactions such as the Bjerknes feedback (Bjerknes, 1969) and the wind-evaporation feedback (Xie, 1998,2004). A southward shift of the ITCZ results in weakened southeasterly cross-equatorial trade winds south of the equator, and thus results in a warming of the cold tongue in the EEP via reduced upwelling and wind-evaporation. Weakened trade winds in the EEP also reduce the westward advection of warm surface seawater, leading to weaker Walker circulation. Because weakened Walker circulation subsequently leads to decreased trade winds in the EEP, this creates a positive feedback mechanism to further amplify the warming of the cold tongue (the Bjerknes feedback). It is important to note that the resultant ocean-atmosphere conditions are likely to lead to a suppression of the annual cycle strength in the EEP and hence an intensification of ENSO variance (Timmermann et al., 2007).

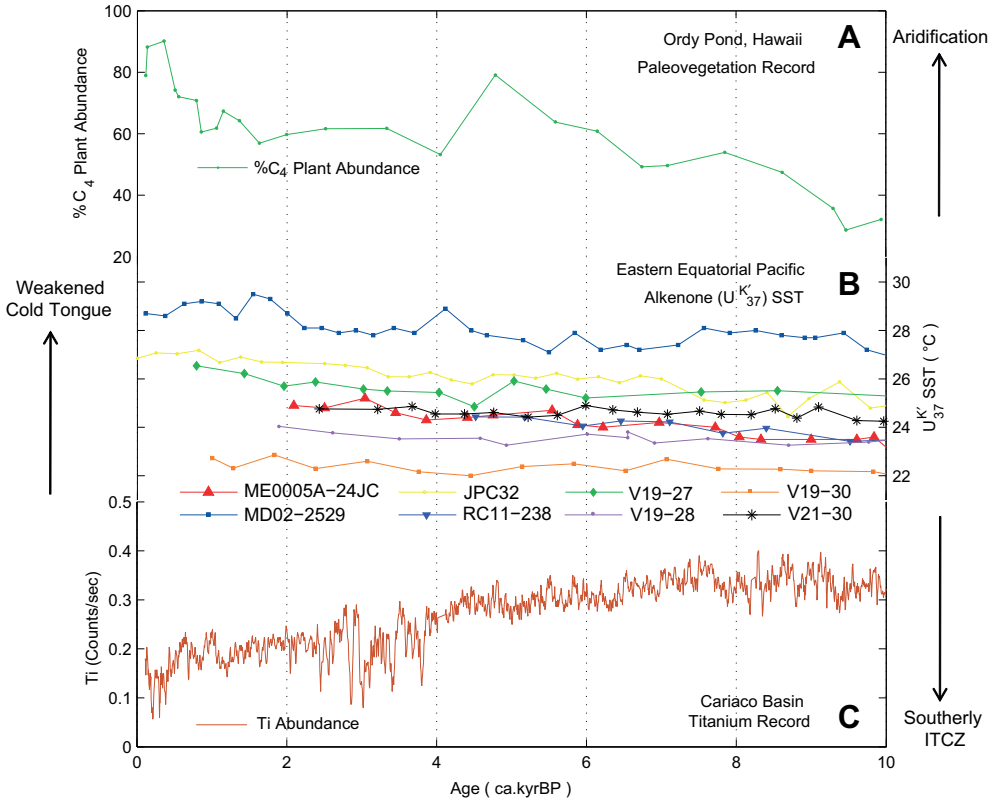

Fig. 5. Comparison of the aridity changes in Hawaii, $U^{K'}_{37}$ derived SST of the cold tongue in the EEP and latitudinal shifts of the ITCZ over the Holocene period. (A) Holocene aridity changes in Hawaii inferred from $\delta^{13}C$ of *n*-alkanes from Ordy Pond, Hawaii (this study). (B) $U^{K'}_{37}$ derived paleo-SST records in the EEP. The data for sites ME0005A-24JC, JPC32 and MD02-2529 are from Kienast et al. (2006), Pahnke et al. (2007) and Leduc et al. (2007), respectively. The data for sites RC11–238, V19–27, V19–28, V19–30 and V21-30 are from Koutavas and Sachs (2008). (C) Titanium record from Cariaco Basin sediments at ODP site 1002 (10° 42.73′ N, 65° 10.18′ W: Haug et al., 2001).

5. Conclusion

The $\delta^{13}C$ record of leaf wax *n*-alkanes from Ordy Pond sediments provides the first continuous Holocene paleoclimate record from Hawaii. The shift of the local vegetation from C_3 to C_4-dominated flora since the early Holocene suggests aridification in Hawaii as a result of reduced wintertime precipitation. Our model simulations revealed a consistent drying trend in the subtropical Pacific as well as concomitant warming of the cold tongue in the EEP in response to the increase in winter insolation along the equator. It is also likely that Holocene southward shift of the ITCZ, at least to some extent, contributed to the weakening of the cold tongue in the EEP via dynamic feedback mechanisms. Alkenone-based Holocene SST records in the EEP and other proxies for paleo-positioning of the ITCZ are consistent with this scenario. We conclude that ocean-atmosphere responses to the warming of the cold tongue in the EEP modulated precipitation patterns in Hawaii by suppressing large-scale moisture supplies as well as the probability of subtropical cyclones via atmospheric adjustments that are similar to the modern-day El Niño-Southern Oscillation teleconnection.

Acknowledgement

This work was funded by Petroleum Research Fund (PRF #40088-ACS) to Schoonmaker. Timmermann was supported by a grant from the NSF paleoclimate program and by the JAMSTEC through its sponsorship of the IPRC. CGCM experiments were conducted with the NEC supercomputer at the German Climate Computing Center (DKRZ). We thank R. Wallsgrove, T. Rust, and J. Tanimoto for technical support. We are grateful to J. Hayes, S. Athens, J. Ehleringer and P.S. Chu for reviews. We also thank the editor and two anonymous reviewers for constructive comments. SOEST contribution number 7975 and IPRC contribution number 711.

References

Athens, J.S., 1997. Hawaiian native lowland vegetation in prehistory. In: Kirtch, P.V., Hunt, P.V. (Eds.), Historical Ecology in the Pacific Islands: Prehistoric Environmental and Landscape Change. Yale University Press, Connecticut, pp. 248–270.

Athens, J.S., 2008. *Rattus exulans* and the catastrophic disappearance of Hawai'i's native lowland forest. Biological Invasions 11, 1489–1501. doi:10.101007/s10530-008-9402-3.

Athens, J.S., Tuggle, H.D., Ward, J.V., Welch, D.J., 2002. Avifaunal extinctions, vegetation change, and Polynesian impacts in prehistoric Hawai'i. Archaeology in Oceania 37, 57–78.

Athens, J.S., Ward, J.V., Blinn, D.W., 2007. Vegetation history of Laysan island, Northwestern Hawaiian Islands. Pacific Science 61, 17–37.

Austin, A.T., Vitousek, P.M., 1998. Nutrient dynamics on a precipitation gradient in Hawaii. Oecologia 113, 519–529. doi:10.1007/s004420050405.

Bi, X., Sheng, G., Liu, X., Li, C., Fu, J., 2005. Molecular and carbon and hydrogen isotopic composition of *n*-alkanes in plant leaf waxes. Organic Geochemistry 36, 1405–1417.

Bjerknes, J., 1969. Atmospheric teleconnections from the equatorial Pacific. Monthly Weather Review 97, 163–172.

Burney, L.P., Burney, D.A., 2003. Charcoal stratigraphies for Kaua'i and the timing of human arrival. Pacific Science 57, 211–226.

Caruso, S.J., Businger, S., 2006. Subtropical cyclogenesis over the central north Pacific. Weather and Forecasting 21, 193–205.

Chadwick, O.A., Kelly, E.F., Hotchkiss, S.C., Vitousek, P.M., 2007. Precontact vegetation and soil nutrient status in the shadow of Kohala Volcano, Hawaii. Geomorphology 89, 70–83.

Chikaraishi, Y., Naraoka, H., 2003. Compound-specific δD-$\delta^{13}C$ analyses of *n*-alkanes extracted from terrestrial and aquatic plants. Phytochemistry 63, 361–371.

Chu, P.-S., 1995. Hawaii rainfall anomalies and El Niño. Journal of Climate 8, 1697–1703.

Collister, J.W., Rieley, G., Stern, B., Eglinton, G., Fry, B., 1994. Compound-specific $\delta^{13}C$ analyses of leaf lipids from plants with differing carbon dioxide metabolisms. Organic Geochemistry 21, 619–627.

Conroy, J.L., Overpeck, J.T., Cole, J.E., Shanahan, T.M., Steinitz-Kannan, M., 2008. Holocene changes in eastern tropical Pacific climate inferred from a Galápagos lake sediment record. Quaternary Science Reviews 27, 1166–1180.

Conte, M.H., Webber, J.C., Carlson, P.J., Flanagan, L.B., 2003. Molecular and carbon isotopic composition of leaf wax in vegetation and aerosols in a northern prairie ecosystem. Oecologia 135, 67–77.

Donders, T.H., Wagner-Cremer, F., Visscher, H., 2008. Integration of proxy data and model scenarios for the mid-Holocene onset of modern ENSO variability. Quaternary Science Reviews 27, 571–579.

Dubois, N., Kienast, M., Normandeau, C., Herbert, T.D., 2009. Eastern equatorial Pacific cold tongue during the Last Glacial Maximum as seen from alkenone paleothermometry. Paleoceanogrpahy 24, PA4207. doi:10.1029/2009PA001781.

Dykoski, C.A., Edwards, R.L., Cheng, H., Yuan, D., Cai, Y., Zhang, M., Lin, Y., Jiaming, Q., An, Z., Revenaugh, J., 2005. A high-resolution, absolute-dated Holocene and deglacial Asian monsoon record from Dongge Cave, China. Earth and Planetary Science Letters 233, 71–86.

Edwards, E.J., Still, C.J., 2008. Climate, phylogeny and the ecological distribution of C_4 grasses. Ecology Letters 11, 266–276.

Ehleringer, J.R., Cerling, T.E., Helliker, B.R., 1997. C_4 photosynthesis, atmospheric CO_2, and climate. Oecologia 112, 285–299.

Ehleringer, J.R., Bowling, D.R., Flanagan, L.B., Fessenden, J., Helliker, B., Martinelli, L.A., Ometto, J.P., 2002. Stable isotopes and carbon cycle processes in forests and grasslands. Plant Biology 4, 181–189.

Ehleringer, J.R., 2005. The influence of atmospheric CO_2, temperature, and water on the abundance of C_3/C_4 taxa. In: Ehleringer, J.R., Cerling, T.E., Dearing, M.D. (Eds.), A History of Atmospheric CO_2 and Its Effect on Plants, Animals, and Ecosystems. Springer Verlag, NY, pp. 214–231.

Epstein, H.E., Lauenroth, W.K., Burke, I.C., Coffin, D.P., 1997. Productivity patterns of C_3 and C_4 functional types in the U.S. Great Plains. Ecology 78, 722–731.

Farquhar, G.D., Ehleringer, J.R., Hubick, K.T., 1989. Carbon isotope discrimination and photosynthesis. Annual Review of Plant Physiology and Plant Molecular Biology 40, 503–537.

Felis, T., Lohmann, G., Kuhnert, H., Lorenz, S.J., Scholz, D., Paetzold, J., Al-Rousan, S.A., Al-Monghrabi, S.M., 2004. Increased seasonality in Middle East temperatures during the Last Interglacial period. Nature 429, 164–168.

Fleitmann, D., Burns, S.J., Mudelsee, M., Neff, U., Kramers, J., Mangini, A., Matter, A., 2003. Holocene forcing of the Indian monsoon recorded in a stalagmite from southern Oman. Science 300, 1737–1739.

Fleitmann, D., et al., 2007. Holocene ITCZ and Indian monsoon dynamics recorded in stalagmites from Oman and Yemen (Socotra). Quaternary Science Reviews 26, 170–188.

Garrison, G.H., 2002. Holocene sedimentary and aquatic biogeochemical responses reflected in Ordy Pond, O'ahu, Hawai'i and contemporary modeling of submarine groundwater discharge in Kahana Bay, O'ahu, Hawai'i. Ph.D. Dissertation, Univ. of Hawai'i., (U.S.A).

Hallam, N.D., 1970. Growth and regeneration of waxes on the leaves of *Eucalyptus*. Planta 93, 257–268.

Haug, G.H., Hughen, K.A., Sigman, D.M., Peterson, L.C., Röhl, U., 2001. Southward migration of the intertropical convergence zone through the Holocene. Science 293, 1304–1308.

Hauke, V., Schreiber, L., 1998. Ontogenetic and seasonal development of wax composition and cuticular transpiration of ivy (*Hedera helix* L.) sun and shade leaves. Planta 207, 67–75.

Hodell, D.A., Curtis, J.H., Jones, G.A., Higuera-Gundy, A., Brenner, M., Binford, M.W., Dorsey, K.T., 1991. Reconstruction of Caribbean climate change over the past 10 500 years. Nature 352, 790–793.

Hotchkiss, S., Juvik, J.O., 1999. A late-Quaternary pollen record from Ka'au Crater, O'ahu, Hawai'i. Quaternary Research 52, 115–128.

Indermühle, A., et al., 1999. Holocene carbon-cycle dynamics based on CO_2 trapped in ice at Taylor Dome, Antarctica. Nature 398, 121–126.

Keeley, J.E., Rundel, P.W., 2003. Evolution of CAM and C_4 carbon-concentrating mechanisms. International Journal of Plant Sciences 164, S55–S77.

Kenig, F., Popp, B.N., Summons, R.E., 2000. Preparative HPLC with ultrastable-Y zeolite for compound-specific carbon isotope analyses. Organic Geochemistry 31, 1087–1094.

Kienast, M., Kienast, S.S., Calvert, S.E., Eglinton, T.I., Mollenhhauer, G., Francois, R., Mix, A.C., 2006. Eastern Pacific cooling and Atlantic overturning circulation during the last deglaciation. Nature 443, 846–849.

Koutavas, A., Lynch-Stieglitz, J., 2003. Glacial-interglacial dynamics of the eastern equatorial Pacific cold tongue-intertropical convergence zone system reconstructed from oxygen isotope records. Paleoceanography 18 (4), 1089. doi:10.1029/2003PA000894.

Koutavas, A., Lynch-Stieglitz, J., 2004. Variability of the marine ITCZ over the eastern Pacific during the past 30 000 years. In: Doaz, H.F., Bradley, R.S. (Eds.), The Hadley Circulation: Present, Past and Future. Kluwer Academic Publishers, Dordrecht, Netherlands, pp. 347–369.

Koutavas, A., Sachs, J.P., 2008. Northern timing of deglaciation in the eastern equatorial Pacific from alkenone paleothermometry. Paleoceanography 23, PA4205. doi:10.1029/2008PA001593.

Leduc, G., Vidal, L., Tachikawa, K., Rostek, F., Sonzogni, C., Beaufort, L., Bard, E., 2007. Moisture transport across Central America as a positive feedback on abrupt climatic changes. Nature 445, 908–911.

Lee, K.E., Slowey, N.C., 1999. Cool surface waters of the subtropical North Pacific Ocean during the last glacial. Nature 397, 512–514.

Lee, K.E., Slowey, N.C., Herbert, T.D., 2001. Glacial sea surface temperatures in the subtropical North Pacific: a comparison of $U^{k'}_{37}$, $\delta^{18}O$, and foraminiferal assemblage temperature estimates. Paleoceanography 16, 268–279.

Legutke, S., Voss, R., 1999. The Hamburg Atmosphere-Ocean Circulation Model ECHO-G: Technical Report. German Climate Computer Center (DKRZ).
Lockheart, M.J., Poole, I., Van Bergen, P.F., Evershed, R.P., 1998. Leaf carbon isotope compositions and stomatal characters: important considerations for paleoclimate reconstructions. Organic Geochemistry 29, 1003–1008.
Lorenz, S.J., Lohmann, G., 2004. Acceleration technique for Milankovitch type forcing in a coupled atmosphere-ocean circulation model: method and application for the Holocene: climate. Dynamics 23, 727–743.
Lorenz, S.J., Kim, J.-H., Rimbu, N., Schneider, R.R., Lohman, G., 2006. Orbitally driven insolation forcing on Holocene climate trends: evidence from alkenone data and climate modeling. Paleoceanography 21, PA1002. doi:10.1029/2005PA001152.
Min, S.-K., Legutke, S., Hense, A., Kwon, W.-T., 2005. Internal variability in a 1000-yr control simulation with the coupled climate model ECHO-G -II. El Niño Southern Oscillation and North Atlantic Oscillation. Tellus A 57, 622–640.
Moy, C.M., Seltzer, G.O., Rodbell, D.T., Anderson, D.M., 2002. Variability of El Niño/Southern Oscillation activity at millennial timescales during the Holocene epoch. Nature 420, 162–165.
NOAA. National Data Centers Climate Data. http://cdo.ncdc.noaa.gov/pls/plclimprod/poemain.accessrouter?datasetabbv=SOD Online (cited on 8th, October 2007).
Otkin, J.A., Martin, J.E., 2004. A synoptic climatology of the subtropical kona storm. Monthly Weather Review 132, 1502–1517.
Pahnke, K., Sachs, J.P., Keigwin, L., Timmermann, A., Xie, S.-P., 2007. Eastern tropical Pacific hydrologic changes during the past 27 000 uears from D/H ratios in alkenones. Paleoceanogrpahy 22, PA4214. doi:10.1029/2007PA001468.
Peterson, L.C., Haug, G.H., 2006. Variability in the mean latitude of the Atlantic intertropical convergence zone as recorded by riverine input of sediments to the Cariaco basin (Venezuela). Palaeogeography, Palaeoclimatology, Palaeoecology 234, 97–113.
Phillips, D.L., Gregg, J.W., 2001. Uncertainty in source partitioning using stable isotopes. Oecologia 127, 171–179.
Rein, B., Lückge, A., Reinhardt, L., Sirocko, F., Wolf, A., Dullo, W.-C., 2005. El Niño variability off Peru during the last 20 000 years. Paleoceanography 20, PA4003. doi:10.1029/2009PA001099.
Rodbell, D.T., Seltzer, G.O., Anderson, D.M., Abbott, M.B., Enfield, D.B., Newman, J.H., 1999. An ¯15,000-year record of El Niño-driven alleviation in southwestern Ecuador. Science 283, 516–520.
Roeckner, E., Arpe, K., Bengtsson, L., Christoph, M., Claussen, M., Duemenil, L., Esch, M., Giorgetta, M., Schlese, U., Schulzweida, U., 1996. The Atmospheric General Circulation Model ECHAM-4: Model Description and Simulation of Present-Day Climate. Technical Report 218. Max Planck Institute for Metrology, Germany.
Rooney, J.J.B., Fletcher, C.H., 2005. Shoreline change and Pacific climatic oscillations in Kihei, Maui, Hawaii. Journal of Coastal Research 21, 535–547.
Sachs, J.P., Sachse, D., Smittenberg, R.H., Zhang, Z., Battisti, D., Golubic, S., 2009. Southward movement of the Pacific intertropical convergence zone AD 1400-1850. Nature Geoscience doi:10.101038/NGEO554.
Shakun, J.D., Burns, S.J., Fleitmann, D., Kramers, J., Matter, A., Al-Subary, A., 2007. A high-resolution, absolute-dated deglacial speleothem record of Indian Ocean climate from Socotra Island, Yemen. Earth and Planetary Science Letters 259, 442–456.
Steinke, S., Kienast, M., Groeneveld, J., Lin, L.-C., Chen, M.-T., Rendle-Bühring, R., 2008. Proxy dependence of the temporal pattern of deglacial warming in the tropical South China Sea: toward resolving seasonality. Quaternary Science Reviews 27, 688–700.
Stowe, L.G., Teeri, J.A., 1978. The geographic distribution of C_4 species of the Dicotyledonae in relation to climate. The American Naturalist 112, 609–623.
Timmermann, A., Lorenz, S.J., An, S.-I., Clement, A., Xie, S.-P., 2007. The effect of orbital forcing on the mean climate and variability of the tropical Pacific. Journal of Climate 20, 4147–4159.
Tribble, J.S., Garrison, G.H., Athens, J.S., Allen, C.B., Skilbeck, C.G., Frankel, E., 1999. Evidence for early-mid Holocene sea-level on O'ahu, Hawai`I from coastal pond sediments. In: Fletcher, C.H., Matthews, J.V. (Eds.), The Non-steady State of the Inner Shelf and Shoreline: Coastal Change on the Timescale of Decades to Millennia in the Late Quaternary. Abstracts with Programs. Inaugural Meeting of IGCP Project #437 "Coastal Environmental Change during the Sea Level Highstand". University of Hawai'I, Honolulu, pp. 9–12. Nov.
U.S. Department of Agriculture Plant Database. http://plants.usda.gov.
Uchikawa, J., Popp, B.N., Schoonmaker, J.E., Xu, L., 2008. Direct application of compound-specific radiocarbon analysis of leaf waxes to establish lacustrine sediment chronology. Journal of Paleolimnology 39, 43–60.
Wagner, W.L., Herbst, D.R., Sohmer, S.H., 1990. Manual of the Flowering Plants of Hawai'i, vol. 1. Bishop Museum Special Publication 83, University of Hawai'i and Bishop Museum Press, Hawaii. 36–119.
Wang, Y., Cheng, H., Edwards, R.L., He, Y., Kong, X., An, Z., Wu, J., Kelly, M.J., Dykoski, C.A., Li, X., 2005. The Holocene Asian monsoon: links to solar changes and north Atlantic climate. Science 308, 854–857.
Wirthensohn, M.G., Sedgley, M., 1996. Epicuticular wax structure and regeneration on developing juvenile *Eucalyptus* leaves. Australian Journal of Botany 44, 691–704.
Xie, S.-P., 1998. Ocean-atmosphere interaction in the making of the Walker circulation and equatorial cold-tongue. Journal of Climate 11, 189–201.
Xie, S.-P., 2004. The shape of continents, air-sea interaction, and the rising branch of the Hadley circulation. In: Diaz, H.F., Bradley, R.S. (Eds.), The Hadley Circulation: Present, Past and Future. Kluwer Academic Publishers, Dordrecht, Netherlands, pp. 121–152.
Yancheva, G., Nowaczyk, N.R., Mingram, J., Dulski, P., Schettler, G., Negendank, J.W., Liu, J.L., Sigman, D.M., Peterson, L.C., Haug, G.H., 2007. Influence of the intertropical convergence zone on the East Asian monsoon. Nature 445, 74–77.